

Relativistic superdense matter in cold systems: Applications*

Richard L. Bowers

*Department of Physics, Texas A & M University, College Station, Texas 77843
and Center for Particle Theory, Physics Department, University of Texas at Austin, Austin, Texas 78712†*

A. M. Gleeson and R. Daryl Pedigo

Center for Particle Theory, Physics Department, University of Texas at Austin, Austin, Texas 78712

(Received 29 May 1975)

The fully relativistic model of the strong interactions between hyperons, described in the preceding paper, is used to investigate the properties of superdense matter. This model can be solved exactly, and the low-temperature limit applied directly to construct neutron star models. Our results lead to a significantly higher mass stability limit ($M_{\max} = 2.39 M_{\odot}$) which has far-reaching implications for black-hole astrophysics. It also yields moments of inertia well above the observational lower bounds for pulsars. The model predicts a phase transition which includes nuclear densities, and which has significant implications for the detailed structure of neutron stars. Despite the low central densities found for stable masses ($\epsilon_c \lesssim 2 \times 10^{15} \text{ g/cm}^3$) all members of the first SU(3)-symmetric octet except the Ξ^- enter as stable constituents. In addition, quarks may be used as fundamental constituents for a species of superdense matter applicable to models of the hyperons. Our results indicate that this approach may be fruitful in explaining such phenomena as precocious scaling and quark confinement.

I. INTRODUCTION

The formalism developed in the preceding paper¹ may be used to investigate the properties of low-temperature systems of strongly interacting relativistic fermions at and above nuclear density. Two cases which are of particular interest are superdense baryon matter, as it is expected to occur in neutron stars, and superdense quark matter, as a possible model of the hyperons. The major formal difference between the two cases involves the type and number of constituents to be considered. In our applications to neutron stars we shall consider a normal Fermi system of baryons from the first SU(3)-symmetric octet universally coupled to phenomenological vector and scalar fields. The zero-temperature equation of state is obtained for several choices of the phenomenological coupling strengths, and from it we construct slowly rotating neutron-star models. We find a maximum stable neutron-star mass of $2.39 M_{\odot}$, and obtain models with $M \gtrsim 1 M_{\odot}$ having moments of inertia $I \gtrsim 10^{45} \text{ g cm}^2$. Our results are assessed in terms of observational evidence and current theories of the late stages of stellar evolution. The implications of the increased upper mass limit for relativistic astrophysics are also described.

As a second application of our approach, we consider a superdense system of quarks as a possible preliminary model of the hyperons. The analysis shows that superdense matter composed of quarks at zero temperature also undergoes a phase transition. The two phases differ in density by at least five orders of magnitude. The higher-density phase begins well above nuclear density.

This allows us to interpret the hyperons as quark droplets which coexist stably with an extremely dilute quark gas. This preliminary model suggests that the formation process may be somewhat easier to handle than complete quark confinement. Extension of this approach to construct a more nearly realistic model is discussed.

The notation used below follows that developed in the preceding paper. When referring to equations discussed there we shall place a "I" after the equation number.

II. COUPLING CONSTANTS

In our preliminary approach to the physics of superdense matter the strong interactions were assumed to arise from exchange of the observed mesons needed to fit relativistic nucleon-nucleon scattering data. This approach, which was based on observed meson masses and coupling constants fitted to high-energy nucleon-nucleon scattering data was found to be unsatisfactory. It did show, however, that a model of the strong interactions could be obtained by coupling the baryons via a phenomenological scalar and vector field. The restriction to two fields is sufficient since we consider only spin- $\frac{1}{2}$ fermions with local couplings. When this is done, it is no longer obvious what coupling constants and masses should be associated with the phenomenological fields.

As should be clear from our discussion of the density expansion in the preceding paper, the relation between the meson-exchange parameter and our phenomenological field couplings is remote at best. Therefore a method for determining the coupling strengths $g_s^2 m_B^2 / \mu_s^2 \pi^2$ and

$g_V^2 m_B^2 / \mu_V^2 \pi^2$ appearing in (AII) must be specified.

Several programs which may be used to fix the coupling strengths were outlined in Sec. VI of the preceding paper. The most appealing method would involve fitting nucleon-nucleon scattering with the effective Lagrangian. This program has been carried out by others, and their results may be incorporated directly to fix the coupling constants and choice of mesons to be exchanged. A less ambitious, though still predictive, approach involves the construction of a simple model of nuclear matter. The coupling strengths may be fitted by requiring that the bulk binding energy per nucleon at nuclear density have a specific value. In this way we find that $g_S^2 m_B^2 / \mu_S^2 \pi^2 = 27.04$ and $g_V^2 m_B^2 / \mu_V^2 \pi^2 = 19.83$ reproduce a binding energy per baryon of -15.74 MeV at $q_{F,N} = q_{F,P} = 1.42 \text{ fm}^{-1}$. These values correspond to our best fit model, and will serve as the basis for much of the remaining discussion.

As emphasized previously, we consider the principle uncertainty in our approach to be that inherent in our simplified model of nuclear matter. Conventional approaches to neutron-star matter suffer from the limitation of inherently containing free parameters, many of which are fitted by independent means. In these cases it is extremely impractical to examine the dependence of the resulting equation of state or neutron-star structure on the fitting program.

In our model all the input uncertainty is lumped into the two coupling strengths. Furthermore since our equation of state may be obtained in analytic form, it is possible to gauge the sensitivity of the results to variation in these parameters.

The results which we obtain serve as bounds on our equation of state, and on the maximum mass and moment of inertia of the corresponding neutron-star models. Since our primary interest is in massive neutron stars in the vicinity of the stability peak, our analysis will focus on the vector coupling $g_V^2 m_B^2 / \pi^2 \mu_V^2$ which dominates the interactions at high densities.

One approach to this question of input uncertainty follows from the observation that the uncertainties in the binding energy and density of nuclear matter lead to uncertainties in the scalar and vector coupling strengths. This will be discussed in the conclusion. We find that deviations from our best fit above are small, and do not alter the qualitative conclusions to be presented below.

A second approach is suggested by the following considerations. If we *arbitrarily* set μ_V equal to the observed ω meson mass, we find that the quantity $g_V^2 m_B^2 / \mu_V^2 \pi^2 = 19.83$ leads to a value of 10.87 for $g_V^2 / 4\pi$. This falls well within the range of the phenomenological values for the ω coupling

from nucleon-nucleon scattering data [9.05 to 15.3 (Ref. 2)]. In fact, reasonable agreement with scattering data may be obtained from values as low as 4.77 or as high as 24.0. We therefore recalculate the equation of state for these additional cases (see Fig. 1): (1) a vector coupling $g_V^2 m_B^2 / \mu_V^2 \pi^2 = 45.5$ corresponding to $g_V^2 / 4\pi \approx 24$; (2) same as (1) with $g_S^2 m_B^2 / \mu_S^2 \pi^2$ adjusted to eliminate the phase transition near nuclear density; (3) our original value of $g_S^2 m_B^2 / \mu_S^2 \pi^2$ and $g_V^2 m_B^2 / \mu_V^2 \pi^2 = 9.04$ corresponding to the lower limit $g_V^2 / 4\pi \approx 4.77$.

We will discuss in the following section the equations of state which result for these values. It is well to stress, however, that such variations serve primarily as illustrations of the mathematical dependence of P and ϵ on the coupling strengths and should not be interpreted as corresponding to any realizable physical system.

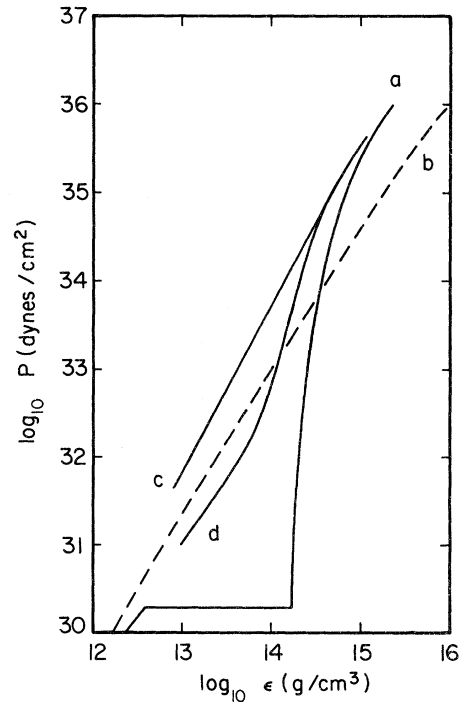


FIG. 1. Dependence of $P(\epsilon)$ on scalar and vector coupling strengths near and above nuclear density. (a) Best-fit equation of state (27.04, 19.83) (the two numbers in parenthesis following each entry in the caption denote values of $g_S^2 m_B^2 / \mu_S^2 \pi^2$ and $g_V^2 m_B^2 / \mu_V^2 \pi^2$, respectively); (b) relativistic ideal neutron gas (0, 0); (c) extreme repulsion obtained if vector coupling constant equals maximum phenomenological ω meson value $g_\omega^2 / 4\pi = 24$ (27.04, 45.5); (d) same as (c), with scalar coupling increased to fit equations of state based on conventional descriptions of nuclear matter for $\epsilon \leq 10^{14} \text{ g/cm}^3$ (52.0, 45.5).

III. BULK PROPERTIES OF SUPERDENSE MATTER

The results of the preceding paper will be applied to determine the equations of state for the $T=0$ system of leptons and baryons given in Table I. This is accomplished in two stages. First, baryon chemical potentials are found from (4.2I) and (3.27I). Chemical equilibrium conditions then determine the densities at which each hyperon species appears in the system. Having found the constituents as a function of total baryon number density, we construct the ground-state energy density and pressure equations of state. Unless otherwise stated, the discussion below will be based on our best-fit model ($g_S^2 m_B^2 / \mu_S^2 \pi^2 = 27.04$ and $g_V^2 m_B^2 / \mu_V^2 \pi^2 = 19.83$).

A. Composition of superdense matter

The particles given in Table I selected as the constituents for our model are the lowest-mass spin- $\frac{1}{2}$ baryons known. Probably the only serious omission in this set is the Δ^{-1} , which because of its low mass and negative charge would be expected to enter between the Λ^0 and Σ^0 .³ The inclusion of spin- $\frac{3}{2}$ particles would require straightforward but significant modification to the approach discussed here. An estimate of the effect of these missing constituents is given with our numerical results. Our equation of state yields matter at low densities, $\epsilon \lesssim 1 \times 10^7$ g/cm³, which consists of nearly free protons and electrons. As the density increases it becomes energetically favorable for protons to undergo e^- capture, with

the simultaneous appearance of a nonzero density of neutrons. At higher densities these weak interactions result in hyperon production. The basic processes involved at $T=0$ for an equilibrium ground state may be written as

$$B(e^-, \nu_e)B' \text{ and } B(\bar{\nu}_e, e^+)B' \quad (3.1)$$

with B and B' suitably chosen members of the first baryon octet. Since the decays (3.1) are weak, the total electric charge Q and baryon number are conserved, and the change in charge and strangeness S of the baryons satisfies $\Delta S = \Delta Q$.

The chemical potentials of the constituent baryons determine the equilibrium composition. In this sense the μ 's act as particle production thresholds. This has been thoroughly discussed in the literature.⁴ The equilibrium conditions on the μ 's which follow from (3.1) are given by Ambartsumyan.⁵ Two dominant mechanisms determine the densities at which various baryons appear. The effective masses, which decrease with increasing density, tend to depress the threshold of each baryonic species. Owing to the presence of e^- in the system, the chemical equilibrium conditions have the opposite effects on the positively charged baryons. Table I summarizes the order in which the baryons appear. The chemical potentials for individual species are shown in Fig. 2. We note that the interacting baryons enter in the same order as they would in a free hyperon gas. The number density of each species is shown in Fig. 3 as a function of the total baryon number density, and the effective masses for selected baryons are shown in Fig. 4.

B. Pressure and energy density

The ground-state energy density is obtained from (4.6I). A particular baryon will contribute a term $\epsilon^{(B)}$ to the total ground-state energy only when the number density n causes the chemical potential $\mu^{(B)}$ to exceed its production threshold. Once the total ground-state energy density $\epsilon = \sum_B \epsilon^{(B)}$ has been found as a function of n , the pressure is obtained from (4.7I) by numerical differentiation. Alternatively (4.4I) and the self-consistency condition (3.27I) may be used. The first approach is numerically the simplest and has been followed here. Representative values of ϵ , P , and n are presented in Table II and Fig. 5. For energy densities $13.40 \leq \log_{10} \epsilon \leq 14.11$ the slope of $P(\epsilon)$ is negative, and for $13.64 \leq \log_{10} \epsilon \leq 14.23$ the system pressure is negative. Throughout this density interval the system contains no hyperons. The dip in pressure indicates that the system possesses two different phases. The pressure P_c at which the phase transition occurs is determined

TABLE I. Particle thresholds. The columns give (1) particle, (2) rest mass in MeV, (3) total baryon-number density (cm⁻³) for which particle appears in the interacting system, (4) same as (3) for free particles, (5) threshold in total baryon energy density (g/cm³). The proton ($m_p = 938.3$ MeV) and electron ($m_e = 0.511$ MeV) are present from zero density.

Particle	Rest mass (MeV)	$10^{-30}n$ (cm ⁻³)		$10^{-15}\epsilon$ (g/cm ³)
		Interacting	Free	Interacting
n	939.6	$\approx 10^{-8}$	$\approx 10^{-8}$	$\approx 10^{-8}$
μ^-	105.7	0.213	0.462	0.369
Σ^-	1197.4	0.245	0.617	0.423
Λ^0	1115.6	0.327	1.22	0.577
Σ^0	1192.5	0.511	3.33	0.950
Ξ^-	1321.3	0.697	3.91	1.43
Σ^+	1189.4	0.712	>6.8	1.48
Ξ^0	1314.9	0.951	>6.8	2.14

by the usual Maxwell construction. P_c may be found by two equivalent means as illustrated in Fig. 6, which shows P versus $1/n$ and μ versus P . In terms of the specific volume $1/n$, P_c is determined by the requirement that the integrals $\int P d(1/n)$ from a to b and from b to c along the curve $P(1/n)$ be equal (the region $P < 0$ is to be included). Alternatively, P_c may be found as the point where the curve for the baryon chemical potential $\mu(P)$ intersects itself, as shown in Fig. 6(b). For present purposes $\mu(P)$ may be replaced by $\mu^{(n)}(P)$ in determining P_c .⁶ We have calculated P_c both ways and find by each method $\log_{10} P_c = 30.336$. The phase transition occurs over the density range $3.44 \times 10^{12} < \epsilon < 1.72 \times 10^{14}$ g/cm³. The bulk modulus of the fluid in each phase is proportional to the slope of $P(\epsilon)$. According to the standard convention the high-density phase will be called a liquid while the lower-density phase will be called a gas. A detailed discussion of the ordering properties of the fluid in each of these phases is outside the scope of the present investigation. Therefore we will retain the simple classifications above for each fluid phase.

At low densities the equation of state approaches

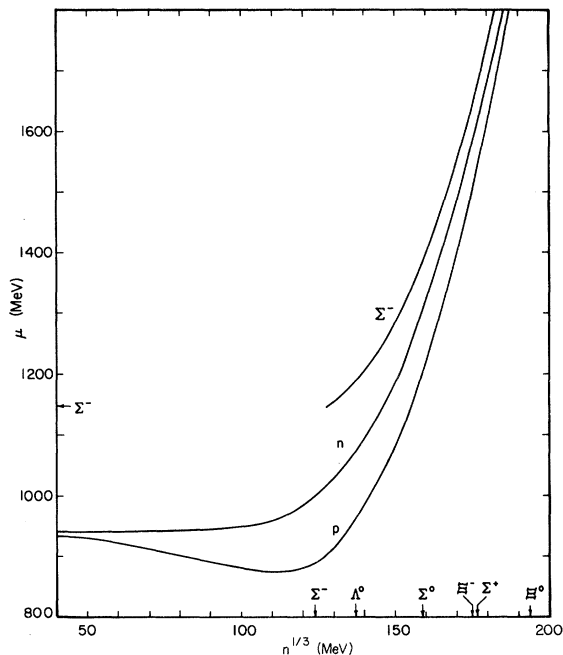


FIG. 2. Baryon chemical potentials in superdense matter vs (total baryon number density)^{1/3}. Arrows on the abscissa indicate hyperon thresholds. The chemical potentials of all similarly charged baryons are equal. The chemical potential for Σ^- below threshold has not been shown. The coupling constants (27.04, 19.83) correspond to best fit.

a free gas. The attractive interactions dominate above the transition region until $\epsilon \approx 1.82 \times 10^{14}$ g/cm³, at which point repulsive effects become significant. At higher densities repulsion dominates, and asymptotically $P \rightarrow \epsilon$ as discussed previously. Hyperon production sets in at the Σ^- threshold, which occurs for $\epsilon \approx 4.23 \times 10^{14}$ g/cm³; the last hyperon in the octet appears when $\epsilon \approx 2.14 \times 10^{15}$ g/cm³.

C. Finite-temperature corrections

An additional feature of our model is that low-temperature corrections which depend only on the $T=0$ equations of state may be easily obtained as described in the preceding paper. Using our best-fit model we have calculated the low-temperature changes in the chemical potential and effective mass for a neutron gas. The results are presented in Table III.

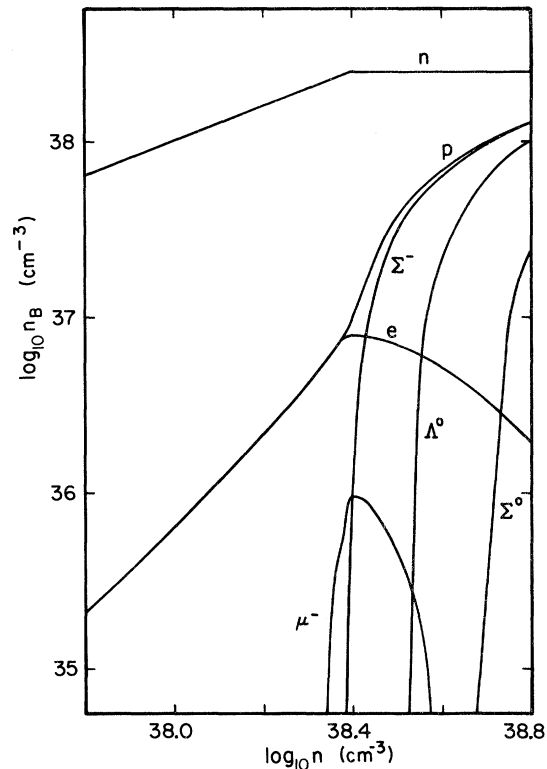


FIG. 3. Particle number densities vs total baryon number density, both in cm⁻³. The hyperon concentrations rise rapidly from zero once their thresholds are exceeded. The μ^- concentration drops to zero for $\log_{10} n_\mu \approx 38.6$. At higher densities there is a tendency for the n 's to approach the same value. The actual threshold density for each hyperon is given in Table I. The coupling constants (27.04, 19.83) correspond to best fit.

D. Variation of coupling strengths

In order to gauge the sensitivity of our results to the choice of scalar and vector coupling strengths we have recalculated $P(\epsilon)$ in the three separate cases discussed in the close of Sec. II. These are illustrated in Fig. 1 along with our best fit a, which has been described above. Curve b is a free gas of neutrons.

Curve c corresponds to the case (1) ($g_V^2 m_B^2 / \mu_V^2 \pi^2 = 45.5$ and $g_S^2 m_B^2 / \mu_S^2 \pi^2 = 27.04$). We observe that at high densities the differences between a and c become quite small, but that c is well above a free gas even at relatively low densities. In particular, there is no evidence of the dominant attractive forces which bind nuclei for $\epsilon \sim 10^{14}$ g/cm³. Although this is not the stiffest equation of state which could result⁷ in principle, it is highly likely that reasonable physical theories

would lead to softer results.

A more nearly acceptable alternative may be reached if the scalar coupling is also increased. The physical motivation in doing so is the simple fact that the attractive interactions dominate in the neighborhood of nuclear density. Curve d results if we require that our equation of state reproduce the equations of state obtained by more conventional methods applied to the regime of nuclear density. This corresponds to case (2) ($g_V^2 m_B^2 / \mu_V^2 \pi^2 = 45.5$ and $g_S^2 m_B^2 / \mu_S^2 \pi^2 = 52.0$). The vector coupling is identical to that used for case (1). Although the fit to conventional equations of state is reasonable for $\epsilon \lesssim 10^{14}$ g/cm³, the corresponding coupling strengths would not be expected to lead to a sensible description of nuclear matter. Notice that there is no phase transition in this case, since in this region the repulsive

TABLE II. Equation of state. The first three columns give the baryon energy density ϵ (g/cm³), pressure P (dyn/cm²), and total number density n (cm⁻³). The last three columns give the proton, neutron, and Σ^- chemical potentials (MeV) in the system. Several entries are given in the region of the phase transition; these values of the pressure, indicated by an asterisk, were replaced by 2.16×10^{30} for the present calculation.

n (cm ⁻³)	ϵ (g/cm ³)	P (dyn/cm ²)	μ^p (MeV)	μ^n (MeV)	μ^{Σ^-} (MeV)
1.396×10^{35}	2.340×10^{11}	3.810×10^{28}	938.2	940.0	...
2.837×10^{35}	4.755×10^{11}	1.159×10^{29}	938.1	940.3	...
6.637×10^{35}	1.113×10^{12}	4.251×10^{29}	937.9	940.7	...
1.142×10^{36}	1.914×10^{12}	9.465×10^{29}	937.6	941.0	...
2.053×10^{36}	3.443×10^{12}	2.165×10^{30}	937.0	941.5	...
3.981×10^{36}	6.681×10^{12}	5.107×10^{30} *	935.9	942.2	...
7.533×10^{36}	1.265×10^{13}	1.014×10^{31} *	933.7	942.7	...
1.372×10^{37}	2.305×10^{13}	1.431×10^{31} *	930.1	943.0	...
2.108×10^{37}	3.542×10^{13}	9.347×10^{30} *	925.9	942.8	...
2.580×10^{37}	4.335×10^{13}	4.798×10^{29} *	923.2	942.6	...
3.981×10^{37}	6.688×10^{13}	-4.673×10^{31} *	915.6	941.7	...
1.010×10^{38}	1.695×10^{14}	-2.086×10^{31} *	887.9	941.4	...
1.027×10^{38}	1.723×10^{14}	2.818×10^{30}	887.3	941.5	...
1.032×10^{38}	1.732×10^{14}	1.132×10^{31}	887.1	941.6	...
1.049×10^{38}	1.760×10^{14}	3.790×10^{31}	886.5	941.7	...
1.088×10^{38}	1.825×10^{14}	1.088×10^{32}	885.2	942.2	...
1.175×10^{38}	1.972×10^{14}	3.216×10^{32}	882.4	943.4	...
1.354×10^{38}	2.272×10^{14}	1.027×10^{33}	877.7	946.9	...
1.625×10^{38}	2.730×10^{14}	3.036×10^{33}	873.4	955.4	...
1.781×10^{38}	2.996×10^{14}	4.868×10^{33}	872.7	962.3	...
2.091×10^{38}	3.530×10^{14}	1.041×10^{34}	875.8	980.4	...
2.464×10^{38}	4.184×10^{14}	2.102×10^{34}	888.8	1010	1131
3.051×10^{38}	5.261×10^{14}	3.790×10^{34}	930.2	1048	1165
3.757×10^{38}	6.621×10^{14}	7.290×10^{34}	1003	1111	1220
4.438×10^{38}	8.021×10^{14}	1.264×10^{35}	1094	1193	1292
5.507×10^{38}	1.044×10^{15}	2.514×10^{35}	1264	1349	1434
5.919×10^{38}	1.146×10^{15}	3.102×10^{35}	1333	1413	1493
6.633×10^{38}	1.333×10^{15}	4.265×10^{35}	1456	1529	1601
7.623×10^{38}	1.617×10^{15}	6.137×10^{35}	1630	1693	1756
8.719×10^{38}	1.966×10^{15}	8.520×10^{35}	1820	1875	1930
1.000×10^{39}	2.419×10^{15}	1.177×10^{36}	2044	2091	2139

interactions are dominant. It is found that a slight further increase in the scalar coupling to $g_S^2 m_B^2 / \mu_S^2 \pi^2 \approx 55$ leads to a narrow phase transition near nuclear density.

Finally, we consider the relatively weak coupling $g_V^2 m_B^2 / \mu_V^2 \pi^2 = 9.04$ corresponding to case (3). The equation of state is qualitatively similar in appearance to curve (a). However, the phase transition which develops is extremely broad. The high-density segment of $P(\epsilon)$ is nearly parallel to (a) but is shifted to the right by about an order of magnitude. The low-density branch corresponds to densities less than or equal to those expected to occur in the center of massive white dwarfs. Clearly the model will not reproduce the properties of nuclear matter, and in all likelihood would predict that no stable neutron stars exist. Since this is in obvious contradiction with astrophysical observations we must conclude that the model based on interpreting the phenomenological scalar and vector fields as, in some sense, equivalent to exchange of observed mesons of scalar and vector character is incorrect.

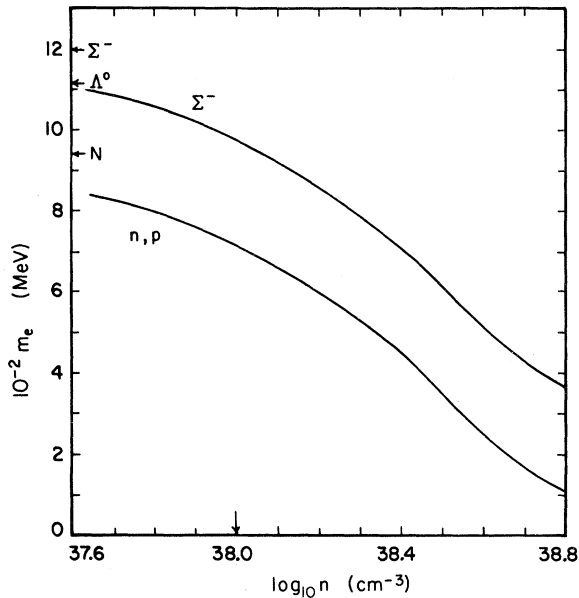


FIG. 4. Representative baryon effective masses (MeV) vs total baryon number density (cm^{-3}). To the scale of the figure the effective mass of the nucleons are equal. The upper curve is for the Σ^- . Note that the baryon m_e 's shift together. The physical rest masses are denoted on the ordinate. The arrow on the abscissa corresponds to nuclear density. The coupling constants (27.04, 19.83) correspond to best fit.

IV. NEUTRON STARS

The $T=0$ equations of state discussed in Sec. III have been used to construct model neutron stars. We present masses, radii, and moments of inertia for slowly rotating neutron stars based on our best-fit model, and compare these with current results.

The method of constructing fully relativistic, slowly rotating neutron stars at zero temperature is well known. This procedure, including a detailed discussion of the numerical program, has been reviewed by Arnett and Bowers.⁸ The essential steps are the following: Einstein's equations for a stationary axially symmetric rigidly rotating medium are expanded about the nonrotating solution.⁹ The star's angular velocity is assumed to be $\Omega \ll \Omega_c = (MG/R^3)^{1/2}$. Expansions in (Ω/Ω_c) are obtained for the moment of inertia I , the gravitational mass M_G , and the mass $M_A \equiv m_A N$, where m_A is the atomic mass unit based on C^{12} and N is the proper baryon number.¹⁰ To within limits set by the uncertainty in any recently constructed

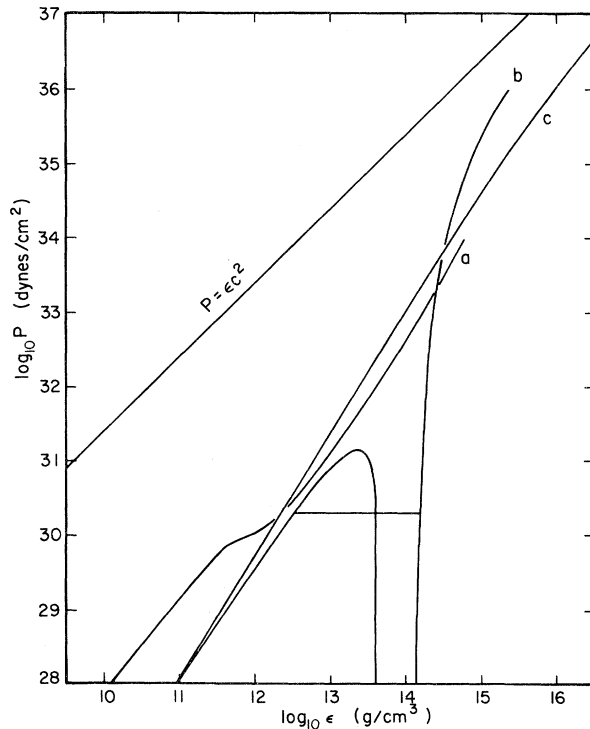


FIG. 5. Equation of state: (a) Baym-Bethe-Pethick and Baym-Pethick-Sutherland equation of state; (b) results of this calculation using coupling constants (27.04, 19.83); (c) free neutron gas. The horizontal line corresponding to $\log_{10} P = 30.34$ represents the phase transition region. The curve labeled "b" asymptotically approaches $P = \epsilon c^2$.

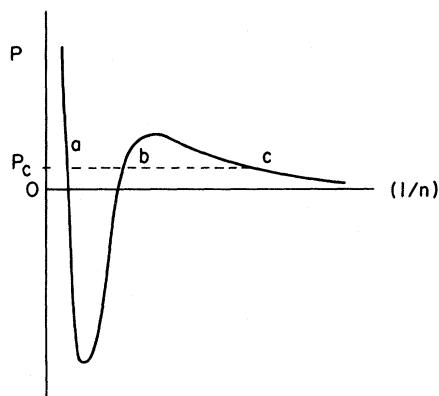
equations of state, including the present model, the corrections to M_G and M_A resulting from rotation are not significant, at least for values of the angular velocity Ω as presently observed in pulsars. For the pulsar in the Crab nebula Ω_{Crab} is approximately 200 sec^{-1} . The moment of inertia, however, does contain terms proportional to Ω/Ω_c which have been retained.

Model neutron stars based on other published equations of state have been surveyed.⁸ The numerical structure program employed here is the same as that used by Arnett and Bowers. Thus our results may be compared directly with the other models as reported there.

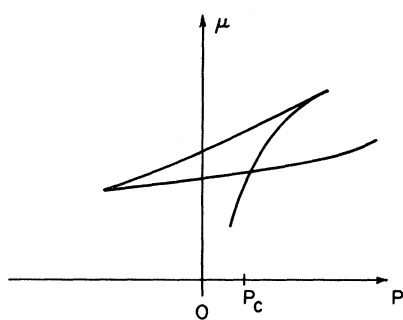
In order to construct neutron-star models an equation of state is needed which covers the density range $\epsilon_s \leq \epsilon < \epsilon_{\text{max}}$, where ϵ_{max} is generally

expected to be in the range 10^{15} – 10^{16} g/cm^3 . The surface density ϵ_s has been taken as 7.86 g/cm^3 (the $T=0$ density of Fe^{56}). Our equation of state could be used throughout the density range above. However, the properties of low-density cold catalyzed matter in neutron stars are well understood. According to current theories, as summarized in Table IV, the least reasonable equation of state at low densities is that of a gas. Therefore we patch to more nearly realistic low-density models below the phase transition. Specifically, the results of Baym, Pethick, and Sutherland¹¹ (BPS) have been used for $\epsilon \leq 2.20 \times 10^{12} \text{ g/cm}^3$. For densities $\epsilon > 1.72 \times 10^{14} \text{ g/cm}^3$ our results have been used.

Selected neutron stars are given in Table V. Each is parametrized by its central density ϵ_c . The mass M_G is shown in Fig. 7 along with models based on the equations of state of Pandharipande¹² and Cameron, Cohen, Langer, and Rosen (CCLR).⁴ The latter treat the interactions non-relativistically. Figure 8 gives M_A as a function of ϵ_c for the same equations of state. The horizontal mark in Fig. 8 gives M_G corresponding to $M_A = 1.41 M_\odot$, and represents the mass of a supernova remnant favored by present evolutionary studies.¹³ Stable neutron stars are those for which



(a)



(b)

FIG. 6. Maxwell construction. (a) Schematic plot of total pressure P vs $1/n$. The dashed line represents the equation of state in the phase transition region. (b) Baryon chemical potential μ vs pressure P . The thermodynamically realized state corresponds to the lowest value of μ . The transition pressure P_c is determined by the intersection of the μ curves for the liquid and gas phases.

TABLE III. Temperature corrections to m_e and μ for neutrons. The coefficients A and B are derived in the previous paper, and have been evaluated for our best fit to nuclear matter as described in Sec. II. Also given is the $T=0$ neutron chemical potential.

$q_{F,N} \text{ (fm}^{-1}\text{)}$	$\mu_N \text{ (MeV)}$	$A \text{ (MeV}^{-1}\text{)}$	$B \text{ (MeV}^{-1}\text{)}$
0.05680	939.7	1.541×10^2	1.664×10^2
0.1420	940.0	2.466×10^1	2.664×10^1
0.2272	940.4	9.630	1.041×10^1
0.3124	941.0	5.084	5.504
0.4260	941.8	2.715	2.947
0.5680	942.6	1.499	1.635
0.7100	943.0	9.272×10^{-1}	1.018
0.8520	942.9	6.095×10^{-1}	6.758×10^{-1}
0.9940	942.2	4.129×10^{-1}	4.642×10^{-1}
1.136	941.2	2.822×10^{-1}	3.234×10^{-1}
1.278	940.5	1.910×10^{-1}	2.252×10^{-1}
1.420	941.4	1.259×10^{-1}	1.547×10^{-1}
1.562	946.1	7.915×10^{-2}	1.038×10^{-1}
1.704	958.8	4.616×10^{-2}	6.739×10^{-2}
1.846	985.9	2.386×10^{-2}	4.216×10^{-2}
1.988	1035	9.885×10^{-3}	2.560×10^{-2}
2.130	1113	1.997×10^{-3}	1.546×10^{-2}
2.272	1220	-2.017×10^{-3}	9.596×10^{-3}
2.414	1355	-3.911×10^{-3}	6.256×10^{-3}
2.556	1516	-4.749×10^{-3}	4.300×10^{-3}
2.698	1701	-5.077×10^{-3}	3.100×10^{-3}
2.840	1908	-5.154×10^{-3}	2.323×10^{-3}

TABLE IV. Composition of cold matter as expected for neutron stars.

ρ (g/cm ³)	Composition
$10^4 - (7 \times 10^6)$	Normal nuclei and nonrelativistic e^-
$(7 \times 10^6) - (4 \times 10^{11})$	Relativistic e^- and Coulomb lattice of increasingly neutron-rich nuclei
$(4 \times 10^{11}) - (2 \times 10^{14})$	Neutron drip; accumulation of free neutrons and nuclear clusters.
$> 2 \times 10^{14}$	Clusters dissolve ; n , p , and e^- Fermi fluids
$> 3 \times 10^{14}$	Hyperon production

$dM/d\epsilon_c > 0$ for both M_A and M_G . Configurations beyond the mass peak are gravitationally unstable and are expected to become black holes.

The maximum stable mass at $T=0$ has, according to our model, a gravitational mass $M_G = 2.39M_\odot$ and $M_A = 2.89M_\odot$, and a central density $\epsilon_c = 2.00 \times 10^{15}$ g/cm³. This represents an increase of as much as 60% over values recently reported in the literature. If supernova remnants are in fact limited to masses M_A lying in a narrow range about $1.41M_\odot$, then the increased maximum mass is expected to have a dramatic effect on the predicted ratio of neutron stars to black holes produced by supernova. In essence, our increased M_{\max} implies that few black holes would be expected to result directly from the late evolutionary stages of isolated stars, and it may reduce the number of neutron stars in close binary systems which become black holes as a result of mass transfer.

Examination of M and R for models in Table V shows an interesting feature. As the mass decreases, the model radius R increases until the

average density of the star falls below $\epsilon \sim 8 \times 10^{14}$ g/cm³. It then decreases with decreasing M until the average ϵ enters the phase transition region. For $\epsilon \lesssim 2.2 \times 10^{12}$ g/cm³ we again find that R increases as M decreases until the mass minimum is reached. The interval $dM/dR > 0$ corresponds to the region where the bulk modulus is large due to the steep slope of the P versus ϵ curve. In fact the star distributes mass in this region as if it were nearly incompressible, the added matter primarily extending the surface while having a small effect on the central density.

Representative energy density profiles are shown in Fig. 9. Also shown are mass fractions for selected models. Of the top three curves, the middle one corresponds to M_{\max} . In these models more than 95% of the stellar matter is at densities greater than nuclear, corresponding to the highly incompressible fluid phase. For this reason the phase transition and the low-density portions of $P(\epsilon)$ have little effect on the structure. The density profiles are nearly flat out to $r=R$ and then drop nearly vertically to $\epsilon = \epsilon_s$. The

TABLE V. Slowly rotating neutron stars. The columns give (a) central density (g/cm³), (b) gravitational mass in solar units ($M_\odot = 1.987 \times 10^{33}$ g), (c) mass M_A in solar units (see Sec. VII, (d) radius (km), (e) moment of inertia (g cm²), and (f) binding energy per baryon (MeV/baryon).

ϵ_c (g/cm ³)	M_G/M_\odot	M_A/M_\odot	R (km)	I (g cm ²)	ϵ_B (MeV/baryon)
2.000×10^{15}	2.39	2.89	11.42	3.05×10^{45}	172.0
1.500×10^{15}	2.33	2.81	11.89	3.13×10^{45}	167.1
1.259×10^{15}	2.24	2.68	12.14	3.05×10^{45}	159.3
1.000×10^{15}	2.02	2.36	12.37	2.70×10^{45}	142.2
8.000×10^{14}	1.68	1.91	12.40	2.12×10^{45}	118.8
7.499×10^{14}	1.57	1.76	12.36	1.92×10^{45}	111.2
6.402×10^{14}	1.28	1.41	12.16	1.45×10^{45}	94.1
6.310×10^{14}	1.26	1.38	12.14	1.41×10^{45}	91.5
5.623×10^{14}	1.06	1.15	11.90	1.10×10^{45}	79.2
4.000×10^{14}	0.540	0.564	10.78	3.93×10^{44}	45.8

V/

lower three curves correspond to models which do feel the phase transition, and are sensitive to the equation of state at low densities. The profiles are remarkably flat up to the phase transition, drop rapidly through this region, and then develop a low-density envelope which balloons to large radii. The latter is due to the BPS equation of state. The sharp falloff in density makes it possible to clearly distinguish the inner core with $\epsilon \gtrsim 1.7 \times 10^{14} \text{ g/cm}^3$ from the envelope for which $\epsilon \lesssim 2.2 \times 10^{12} \text{ g/cm}^3$. The high-density portion of the profiles are extremely flat out to the transition region, and account for nearly all of the mass of the star.

Moments of inertia have also been calculated for the neutron stars in Table V. We find that the maximum moment of inertia occurs at ϵ_c of $1.5 \times 10^{15} \text{ g/cm}^3$, and has the value $I_{\text{max}} = 3.13 \times 10^{45} \text{ g cm}^2$. Furthermore stable models with masses in the range $M \gtrsim 1M_\odot$ have moments of inertia greater than 10^{45} g cm^2 . The maximum moment of inertia occurs at lower density than M_{max} as shown in Fig. 10. Also shown are mo-

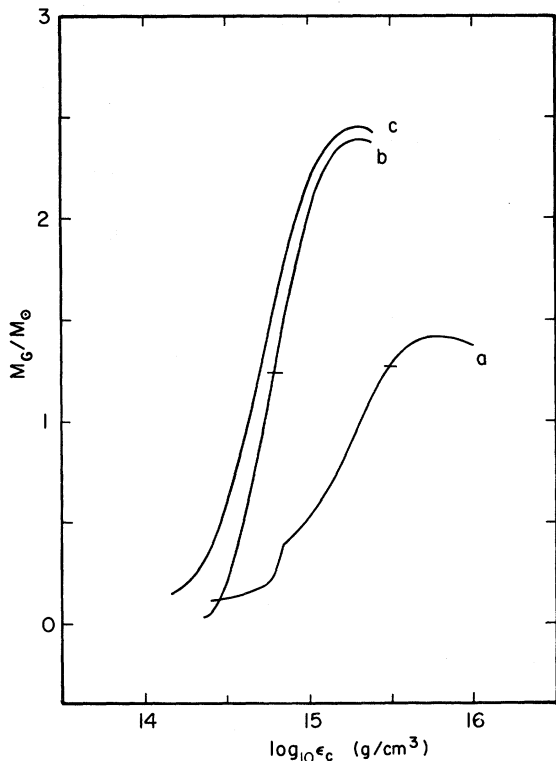


FIG. 7. M_G vs ϵ_c for slowly rotating neutron stars. Curves (a) and (b) are described in Fig. 5. Curve (c) represents the CCLR equation of state. The horizontal slashes indicate the mass M_G corresponding to a remnant mass $M_A = 1.41M_\odot$. Curve (a) for $\epsilon_c > 10^{15} \text{ g/cm}^3$ is obtained from Pandharipande's equation of state for hyperon matter.

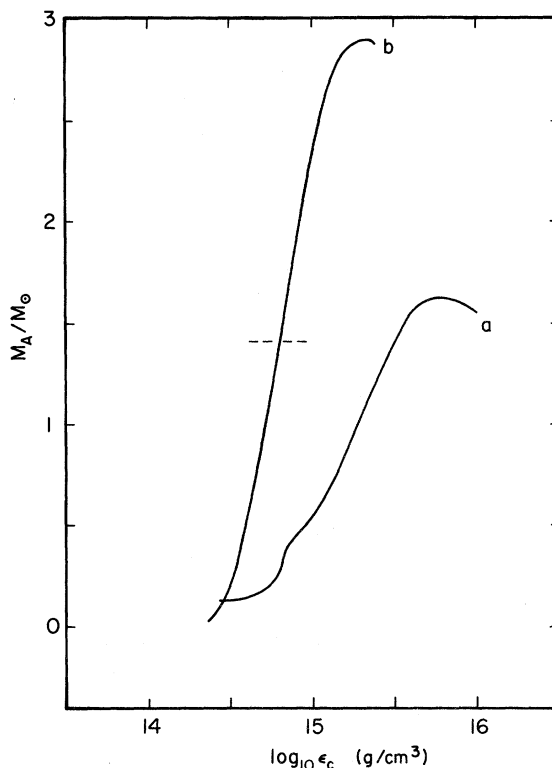


FIG. 8. M_A vs ϵ_c for slowly rotating neutron stars. The treatment follows Fig. 7, except that the CCLR results have been omitted. The slash corresponds to $M_A = 1.41M_\odot$.

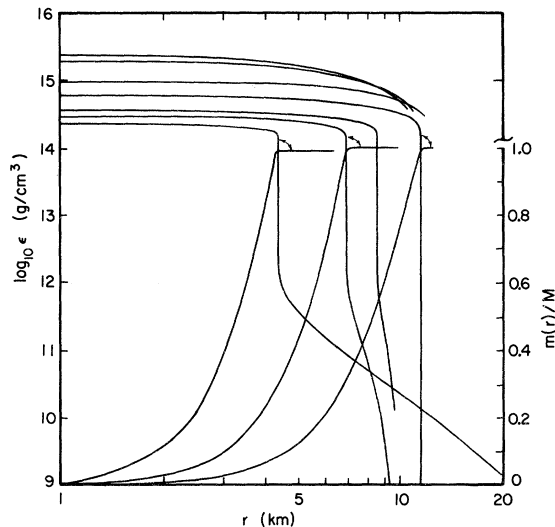


FIG. 9. Energy-density profiles for selected neutron star models (left-hand side scale). Note pronounced core for intermediate mass models. Three gravitational mass fraction curves are also shown (right-hand side scale). The arrow indicates the corresponding density profile. The extended envelopes are seen to contribute negligible mass to the system.

ments of inertia based on the nonrelativistic equations of state of Pandharipande and of CCLR.

The two dashed horizontal lines in Fig. 10 represent the region in which Trimble and Rees¹⁴ place the lower bound on the moment of inertia for the pulsar in the Crab nebula. Their estimate is based on the nebula's luminosity. Considerations of additional observational data¹⁵ suggest that the lower bound may approach 10^{45} g cm², in which case most neutron-star models based on nonrelativistic equations of state could be ruled out since they tend to yield $I_{\text{max}} < 10^{45}$ g cm². In fact, the relatively high values of I for our model appear to be favored by estimates based on current observational data.

Our equation of state contains several features which bear directly on the internal structure of neutron stars. One is the clear distinction between the core and the crust. This follows from the essentially discontinuous change in density at the phase transition, which occurs over nearly two orders of magnitude in density and at a pressure which corresponds closely with the pressure associated with neutron drip. In our model the phase transition is clearly identified with the formation of nuclear matter—a highly incompressible

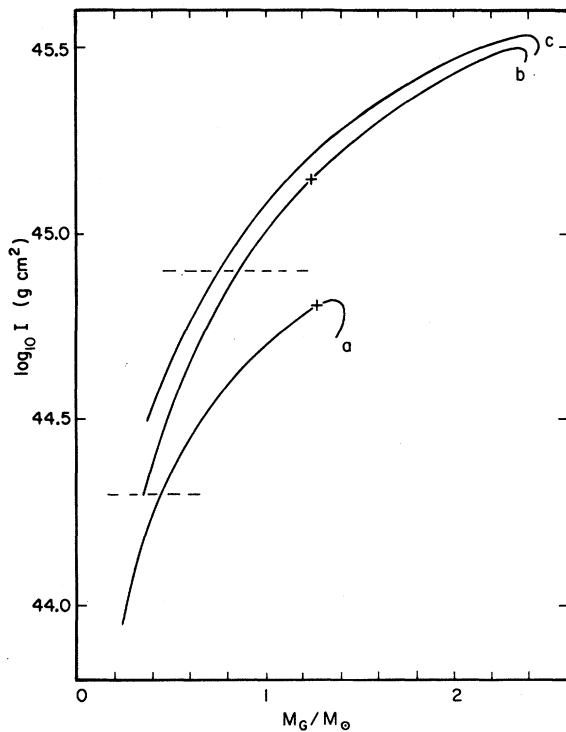


FIG. 10. Moment of inertia vs M_C . Treatment follows Fig. 5. The + denotes the model with $M_A = 1.41M_\odot$. The range in the lower bound on I_{Crab} is shown by the dashed lines.

fluid—and therefore changes the usual mechanism for the smaller phase transition known as neutron drip. In our case the lattice of nuclear clusters is no longer viewed as vaporizing into a nucleon gas phase, but directly dissolving into the nuclear fluid as density increases. This direct, single transition from crystallized nuclear clusters into nuclear fluid provides a marked distinction between the low-density matter in the envelope and the high-density core. The development of an outer phase is thus a natural consequence of the physics of the core. This modified picture of neutron-star structure will have far-ranging consequences for such phenomena as star quakes, couplings to magnetospheres, possible differential rotation rates, and the dynamic formation process itself.

Experience with neutron stars based on nonrelativistic equations of state indicates that an increased maximum stable mass due to increased repulsion is associated with a reduction in core density. Associated with this is a tendency toward fewer hyperon species. In the CCLR model ($M_{\text{max}} = 2.45M_\odot$ and $\epsilon_c = 1.99 \times 10^{15}$ g/cm³) the only hyperons which actually contribute to the equation of state are the Σ^- , Λ^0 , and Δ^- , the latter of which enters essentially at maximum mass. The remaining hyperons in the octet appear at significantly higher densities corresponding to unstable stellar equilibrium. Our equation of state shows nearly the same degree of repulsion as found in CCLR, and the maximum-mass model occurs at practically the same density ($\epsilon_c = 2 \times 10^{15}$ g/cm³). However, all members of the octet, with the exception of the Ξ^0 , contribute to the structure. This may be understood by examining the way in which the scalar and the vector interactions influence the equation of state and the particle thresholds. The relative stiffness of the pressure-energy density curve is due almost entirely to the vector coupling, which dominates the scalar attraction above $\epsilon = 2 \times 10^{14}$ g/cm³. The thresholds, however, are most strongly influenced by the self-consistency requirement which drives the heaviest baryon's m_e asymptotically to zero with increasing density ($m_e, \pi^- \sim 400$ MeV when $\epsilon \sim 2 \times 10^{15}$ g/cm³) as shown in Fig. 6. This effectively increases the number of species that occur at a given density.

A complete analysis of the relation between observational data and the structural implications of this model are beyond the scope of this paper but will be reported elsewhere.

V. CONCLUSION

When the scalar and vector couplings were fitted to nuclear matter in Sec. II we observed that the

greatest uncertainty in our model reflected that which was inherent in our description of nuclear matter. There we assumed $E_B = -15.75$ MeV/baryon at a nuclear density parametrized by $q_{F,N} = 1.42 \text{ fm}^{-1}$. However, these values depend on the way in which the bulk properties of nuclei are extracted from experimental data. Values of E_B used in published models vary in the range $-15.3 > E_B > -16.5$ (Ref. 16). Quoted values of $q_{F,N}$ are equally uncertain.¹⁷

In order to test the sensitivity of our model we varied our values of E_B and $q_{F,N}$ by $\pm 2\%$ and re-determined g_S^2/μ_S^2 and g_V^2/μ_V^2 . The variation in binding energy at fixed $q_{F,N}$ leaves the coupling constants unchanged to three significant figures. Thus to within the limits of currently accepted values these variations may be ignored. Variation in $q_{F,N}$ has a more significant effect on the equation of state. A 2% uncertainty shifts the value of the vector and scalar couplings by about 5%. We estimate that the neutron-star stability limit will also change by about 2%, but in the direction opposite to $q_{F,N}$. Therefore the 2% uncertainty in $q_{F,N}$ implies approximately a $0.05M_\odot$ uncertainty in M_{max} .

We have included the baryons from the first SU(3)-symmetric octet as possible constituents in our treatment of superdense matter. Threshold considerations show that the lowest-mass pion-nucleon resonances should also be included. It is most likely that of these only the Δ^- and Δ^0 need to be considered. The former probably enters at about the same density as the Λ^0 , while the Δ^0 would be expected to follow the Σ^0 .³ We have not included these resonances for two reasons: (1) kinematical complication associated with spin- $\frac{3}{2}$ propagators and (2) these couplings lead to phenomenological tensor-meson exchange which would be difficult to determine from the physics of nuclear matter. We do not feel that a detailed treatment of these added constituents would greatly modify our general conclusions. For models with $\epsilon_c < 5 \times 10^{14} \text{ g/cm}^3$ the results of Sec. IV would remain unchanged. For models having higher central densities we can estimate the possible importance of the resonances by treating them as additional fermions in the system. Experience with neutron-star models shows that the addition of a few extra fermion species results in a pressure decrease typically on the order of 10%.

Non-normal ground states such as superconductivity, superfluidity, pion condensation, ferromagnetism, and crystal structure may play an important role in determining the properties of superdense matter.¹⁸ These effects may be incorporated in our approach by modifying the boundary conditions imposed on the Green's func-

tions. It is probable that the first two effects have only a small influence on P and ϵ for static configurations, and thus should not produce substantial changes in our mass limit. Arguments based on nonrelativistic models of normal superfluids scaled to the regime of nuclear densities imply¹⁹ that if super effects do arise, the gap in the excitation spectrum should close when the density reaches 10^{15} g/cm^3 . Since the maximum central density obtained in our model is $2 \times 10^{15} \text{ g/cm}^3$, it is possible that these effects persist into the core. Because at least seven baryons enter at these densities, it may be possible that each contributes a super phase.

Pion condensation and related phenomena²⁰ are also interesting processes since the reactions $e^- \rightarrow \pi^- + \nu_e$ and $\mu^- \rightarrow \pi^- + \nu_\mu$ can occur at high densities and can carry off an impressive fraction of the star's energy. Physical π^- can be produced only when $\mu_e = \mu_{\pi^-}$. Using the physical value of the pion mass as the chemical potential of a $T=0$ condensed boson state μ_e would have to exceed 140 MeV for production to occur. At all densities in our model $\mu_e < 125$ MeV. However, it should be clear from our results that there are possible interaction effects which could substantially reduce the pion effective mass. The universal scalar-meson coupling would have an effect on the π -meson propagators similar to that found in the case of the baryons. The baryon m_π 's were decreased by about 800 MeV at densities on the order of 10^{15} g/cm^3 . It is not difficult to imagine that the pion effective mass, even if coupled weakly, may be greatly reduced at similar densities. As this happens the e^- and μ^- decay modes shift towards pion production. Real π^- will then appear as a condensate, reducing the system pressure. Since this will only affect the lepton pressure, which is negligible compared to the baryon pressure, π^- condensates will not have a large direct effect on static neutron-star structure. Table VI summarizes the important physical

TABLE VI. Summary of neutron-star structure. The three models listed are (a) the critical model representing the most massive stable neutron star, (b) the model having maximum moment of inertia, and (c) the model whose "remnant" mass $M_A = 1.41M_\odot$.

	M/M_\odot	R (km)	$10^{-45}I(\text{g cm}^2)$
Critical model	2.38	11.42	3.05
Maximum moment of inertia	2.33	11.89	3.13
Remnant model ($M_A = 1.41M_\odot$)	1.28	12.16	1.45

parameters for selected neutron-star models.

The strongly interacting particles are another candidate for a physical realization of cold superdense matter. There are clear experimental indications that these hyperons are composed of a sea of objects which interact locally with an external current, have spin $\frac{1}{2}$ and obey statistics which are either Fermi or para-Fermi.²¹ These objects, called quarks, carry with them the internal symmetries which are manifested by the strongly interacting particles. They are expected to be confined within the hyperons by interactions very similar to those which manifest themselves between the hyperons. They are confined at energies and densities which are clearly relativistic. Furthermore, there are indications of phenomena in particle physics which require a many-body theory for their description.²² It is therefore appropriate that we discuss the applicability of our approach to this problem. The study of superdense matter yields predictions which cannot be obtained from the study of systems comprised of only a few particles.

Only a slight modification of the formal approach which we have developed to treat superdense matter in neutron stars will be required in order to develop a preliminary model of the hyperons. In fact the formal approach of the previous paper may be carried over directly to describe a simple quark model of the hyperons. In order to explore the feasibility of this approach we take as elementary constituents three quark species, each having mass $m_Q = 6$ GeV.²³ We assume that each quark species couples with a universal scalar and vector coupling to baryon number with strengths determined by our previous analysis. In treating the many-body aspect of the problem, the quarks are described by the usual Fermi many-body propagator (2.5I) with m_B replaced by m_Q . The effect of para-Fermi statistics would lead only to a change in the degeneracy factor of order unity. Each type of quark is thus considered to have kinematic and collective properties similar to that of a massive spin- $\frac{1}{2}$ fermion. The model is now completely specified.

Proceeding as in Sec. VI of the preceding paper, we solved for the quark binding energy which reached its minimum value $E_B = -535$ MeV for a quark number density $n \sim 7 \times 10^{39}$ cm⁻³. This is nearly 40 times the number density for which the nuclear binding energy is a minimum. The quark effective masses $m_{e,Q}$ and the chemical potentials were found to have the same qualitative appearance as those of the baryons. The decrease in $m_{e,Q}$ is impressive, reaching a value $m_{e,Q} = 1100$ MeV at minimum binding energy. This effect alone could provide the explanation for the pre-

cocious scaling observed in the high-energy phenomena.²⁴

Finally, we obtained the equation of state which is qualitatively similar to our hyperon equation of state. Further analysis, though, yields a Maxwell construction which occurs at a negative critical pressure. This is indicative of a system possessing a single condensed phase. It is possible that an analysis at finite temperature would produce two stable phases similar to our baryon results. The lower-density phase would be identified as an interacting quark gas, and the high-density phase, a fully condensed liquid, would be the only one surviving at $T=0$. The minimum density for liquid quark matter in the model is 7.0×10^{16} g/cm³.

In order to apply the model to hadronic matter it will be necessary to investigate these phases in detail. We have in mind a liquid-droplet picture with the droplets being associated with baryons in equilibrium with a quark gas phase. The preliminary analysis above indicates that this simple picture is not consistent. The model indicates that a fully condensed fluid phase is the natural $T=0$ state of a quark sea, and that cold droplets can be produced only by some additional formation mechanism. In other words, we find that quark confinement appears to be less difficult to explain than the formation process. However, if we construct a droplet of liquid quark matter at the minimum stable density and confine it to a volume derived from the proton Compton wavelength, the enclosed mass is 2.7×10^{-24} g. It is remarkable that this corresponds roughly to a proton mass.

In order to obtain complete quark confinement within the droplets we would require additional physical mechanisms. One possible mechanism would utilize surface binding. It is notable that this is the mechanism of nuclei formation. Our model of nuclear matter is also found to possess only a liquid phase at zero temperature. A consistent description of atomic nuclei would then require the incorporation of additional formation mechanisms. A second and more interesting mechanism can be inferred from our discussion of pion condensation in neutron stars. If the meson exchanges which are responsible for our fundamental interactions are also composed of quark constituents coupled universally to baryon number, these mesons will have their effective masses reduced significantly, possibly even to zero. In this context the vector-meson octet could provide us with a candidate for a Yang-Mills non-Abelian vector gauge field. This field would be the source of an infrared catastrophe, and could thus lead to complete confinement. A

fuller treatment of the implications of our model of superdense matter to elementary particle physics will appear separately.

A final observation concerns the applicability of our approach to symmetry-breaking effects and the masses of elementary particles. The formalism includes finite-temperature effects, and may be used to study particle effective masses at high densities and high temperatures. In this regime it is possible that m_e approaches zero, and that a critical temperature exists below which

specific masses "freeze out" to form a particle spectrum. Examination of these problems will require additional development of the finite temperature effects on the meson propagators.

ACKNOWLEDGMENT

One of the authors (A. M. G.) would like to thank the Aspen Center for Physics for providing an atmosphere for research in which some of this work took place.

*Work supported by the U. S. Atomic Energy Commission under Contract No. AT(40-1) 3992.

†Present address.

¹R. L. Bowers, A. M. Gleeson, and R. D. Pedigo, preceding paper, *Phys. Rev. D* **12**, 3043 (1975).

²K. Erkelenz, *Phys. Rep.* **13C**, 191 (1974).

³This estimate is based on chemical equilibrium of noninteracting baryons, but is also consistent with the results of nonrelativistic models which include interactions.

⁴J. M. Cohen, W. D. Langer, L. C. Rosen, and A. G. W. Cameron, *Astrophys. Space Sci.* **6**, 228 (1970).

⁵V. A. Ambartsumyan, *Astron. Zh.* **37**, 193 (1960) [*Sov. Astron.* **4**, 187 (1960)].

⁶This replacement is, in fact, exact since the baryon and neutron chemical potentials in neutral systems in chemical equilibrium are identical.

⁷A. G. Sabbadini and J. B. Hartle, *Astrophys. Space Sci.* **25**, 117 (1973).

⁸W. D. Arnett and R. L. Bowers, The Univ. of Texas at Austin Publication in Astronomy No. 9, 1974 (unpublished report).

⁹J. B. Hartle, *Astrophys. J.* **150**, 1005 (1967).

¹⁰The masses are discussed in Ref. 8.

¹¹G. Baym, G. Pethick, and P. Sutherland, *Astrophys. J.* **170**, 299 (1971).

¹²V. Pandharipande, *Nucl. Phys.* **A178**, 123 (1971); **A174**, 641 (1971).

¹³W. D. Arnett, *Astrophys. J.* **194**, 373 (1974); **195**, 727 (1975).

¹⁴V. Trimble and M. Rees, *Astrophys. Lett.* **5**, 93 (1970).

¹⁵G. Borner and J. M. Cohen, *Astrophys. J.* **185**, 959 (1973).

¹⁶W. D. Meyers and W. J. Swiatecki, *Nucl. Phys.* **81**, 1 (1966); P. A. Seeger and W. M. Howard, Los Alamos

Scientific Laboratory Report No. LA-5750, 1974 (unpublished).

¹⁷L. R. B. Elton, *Nuclear Sizes* (Oxford Univ. Press, London, 1961); J. W. Negele, *Phys. Rev.* **61**, 1260 (1970); H. A. Bethe, *Annu. Rev. Nucl. Sci.* **21**, 93 (1971).

¹⁸*Physics of Dense Matter: Proceedings of the 53rd Symposium of the International Astronomical Union, Boulder, 1972*, edited by C. J. Hansen (Reidel, Boston, 1974).

¹⁹V. L. Ginzburg, *Usp. Fiz. Nauk* **97**, 601 (1969) [*Sov. Phys.—Usp.* **12**, 241 (1969)].

²⁰R. Sawyer, *Phys. Rev. Lett.* **29**, 382 (1972); A. B. Migdal, *ibid.* **31**, 257 (1973).

²¹There is a vast literature in which these ideas are given and surveyed. Since we cannot list even partially the principal references, we list here some recent review articles: F. Gilman, in *The Strong Interactions*, SLAC Summer Institute in Particle Physics, 1974, edited by M. C. Zipf (National Technical Information Service, U. S. Dept. of Commerce, Springfield, Virginia, 1974); R. P. Feynman, summary talk given at International Conference on Neutrino Physics and Astrophysics Philosophy, 1974 (unpublished); *The Johns Hopkins University Workshop on Current Problems in High Energy Particle Theory*, edited by G. Domokos *et al.* (Johns Hopkins Univ., Baltimore, 1974).

²²E. L. Feinberg, *Phys. Rep.* **5C**, 237 (1972), and references contained therein.

²³The quark mass is as yet undetermined but there are indications that it must be at least this large. J. J. J. Kokkedee, *The Quark Model* (Benjamin, New York, 1969); Y. S. Kim and N. Kwak, *Fields and Quanta* **3**, 1 (1972).

²⁴R. Slansky, *Phys. Rep.* **11C**, 99 (1974), and references contained therein.